

# P–N Junction Passivation in Kesterite Solar Cells by Use of Solution-Processed $\text{TiO}_2$ Layer

Samaneh Ranjbar, Afshin Hadipour, Bart Vermang, Maria Batuk, Joke Hadermann, Siddhartha Garud, Sylvester Sahayaraj, Marc Meuris, Guy Brammertz, Antonio F. da Cunha, and Jef Poortmans

**Abstract**—In this work, we used a solution-processed  $\text{TiO}_2$  layer between  $\text{Cu}_2\text{ZnSnSe}_4$  and CdS buffer layer to reduce the recombination at the p–n junction. Introducing the  $\text{TiO}_2$  layer showed a positive impact on  $V_{OC}$  but fill factor and efficiency decreased. Using a KCN treatment, we could create openings in the  $\text{TiO}_2$  layer, as confirmed by transmission electron microscopy measurements. Formation of these openings in the  $\text{TiO}_2$  layer led to the improvement of the short-circuit current, fill factor, and the efficiency of the modified solar cells.

**Index Terms**— $\text{Cu}_2\text{ZnSnSe}_4$  (CZTSe), kesterite solar cells, p–n junction passivation, solution-processed  $\text{TiO}_2$ .

## I. INTRODUCTION

**K**ESTERITE  $\text{Cu}_2\text{ZnSn}(\text{S},\text{Se})_4$  (CZTSSe) solar cells are being investigated as a cost effective alternative for highly efficient  $\text{Cu}(\text{In},\text{Ga})(\text{S},\text{Se})_2$  (CIGS) solar cells. In kesterite compounds, earth abundant Zn and Sn elements replace rare In and Ga in chalcopyrite CIGS. Despite promising optoelectronic properties of kesterite such as high absorption coefficient and ideal band gap, the performance of kesterite solar cells is still lower than the commercial level. A large open-circuit voltage ( $V_{OC}$ ) deficit from the bandgap ( $E_g/q - V_{OC}$ ) due to the bulk and interface recombination is reported in kesterite solar cells. The bulk recombination in kesterite absorber layer is due to the tail states and potential fluctuations in the bands [1], [2]. The recombination at the Mo rear interface and kesterite/buffer layer junction is also considered as a possible source of  $V_{OC}$  loss. There are two main concerns about these interfaces: 1) band alignments at the Mo/absorber layer interface [3], [4] and absorber layer/buffer layer junction [5], [6]; 2) decomposition reactions during the fabrication process that occur at the Mo rear interface [7], [8] and at the top surface of kesterite absorber layer [9]. According to the theoretical calculations by Minemoto *et al.* [6] the conduction band offset between the CIGS absorber layer and buffer layer has a crucial impact on the electrical parameters of CIGS solar cells. Based on this study a negative offset, also called cliff-like band alignment, in which the conduction band of the buffer layer is lower than the one of the absorber layer decreases  $V_{OC}$  in CIGS/CdS solar cells. This negative offset is a barrier for injected electrons under forward bias that leads to accumulation of injected electrons and increasing the recombination. On the other hand, a positive offset, known as a spike-like conformation, is not a barrier for injected electrons but for photogenerated electrons. If this positive offset is below 0.4 eV, photogenerated electrons can pass the barrier through the thermionic emission but when it is higher than 0.4 eV, it suppresses the transition of photogenerated electrons leading to the decrease of  $J_{SC}$  and FF [6]. The band alignment between  $\text{Cu}_2\text{ZnSnSe}_4$  (CZTSe) and CdS is reported to be a spike-like band alignment with an offset value of 0.48 [5] or 0.34 eV [10] that is almost near to the optimum value.

Decomposition reactions during the fabrication process of kesterite absorber layer lead to the poor quality of the interfaces.

Manuscript received December 7, 2016; revised February 28, 2017; accepted April 3, 2017. This work was supported in part by the European Union's Horizon 2020 research and innovation program under Grant 640868, in part by the Flemish government, Department Economy, Science and Innovation, in part by the FEDER funds through the COMPETE 2020 Programme, and in part by the National Funds through FCT – Portuguese Foundation for Science and Technology under the project UID/CTM/50025/2013. The work of S. Ranjbar was supported by the Portuguese Science and Technology Foundation through Ph.D. grant SFRH/BD/78409/2011. The work of B. Vermang was supported by the Flemish Research Foundation FWO (mandate 12O4215N). (Corresponding author: Samaneh Ranjbar.)

S. Ranjbar is with the Imec – Partner in Solliance, Leuven 3001, Belgium, with the Department of Electrical Engineering, KU Leuven, Heverlee 3001, Belgium, with the Imec Division IMOMECE – Partner in Solliance, Diepenbeek 3590, Belgium, and also with the I3N - Departamento de Física, Universidade de Aveiro, Aveiro 3810-193, Portugal (e-mail: samanehranjbar@gmail.com).

A. Hadipour is with the Imec – Partner in Solliance, Leuven 3001, Belgium (e-mail: Afshin.Hadipour@imec.be).

B. Vermang is with the Imec – Partner in Solliance, Leuven 3001, Belgium, with the Department of Electrical Engineering, KU Leuven, Heverlee 3001, Belgium, with the Imec Division IMOMECE – Partner in Solliance, Diepenbeek 3590, Belgium, and also with the Institute for Material Research, Hasselt University, Diepenbeek 3590, Belgium (e-mail: bart.vermang@imec.be).

M. Batuk and J. Hadermann are with the Electron Microscopy for Materials Science, University of Antwerp, Antwerp 2020, Belgium (e-mail: maria.batuk@uantwerpen.be; Joke.Hadermann@uantwerpen.be).

S. Garud is with the Imec – Partner in Solliance, Leuven 3001, Belgium, with the Department of Electrical Engineering, KU Leuven, Heverlee 3001, Belgium, with the Imec Division IMOMECE – Partner in Solliance, Diepenbeek 3590, Belgium, and also with the Delft University of Technology, Delft 2628 CD, The Netherlands (e-mail: Siddhartha.Garud.ext@imec.be).

M. Meuris and G. Brammertz are with the Imec Division IMOMECE – Partner in Solliance, Diepenbeek 3590, Belgium, and also with the Institute for Material Research, Hasselt University, Diepenbeek 3590, Belgium (e-mail: marc.meuris@imec.be; guy.brammertz@imec.be).

A. F. da Cunha is with the I3N - Departamento de Física, Universidade de Aveiro, Aveiro 3810-193, Portugal (e-mail: antonio.cunha@ua.pt).

S. Sahayaraj and J. Poortmans are with the Imec – Partner in Solliance, Leuven 3001, Belgium, with the Department of Electrical Engineering, KU Leuven, Heverlee 3001, Belgium, with the Imec Division IMOMECE – Partner in Solliance, Diepenbeek 3590, Belgium, and also with the Institute for Material Research, Hasselt University, Diepenbeek 3590, Belgium (e-mail: Jef.Poortmans@imec.be; Sylvester.Sahayaraj@imec.be).

Color versions of one or more of the figures in this paper are available online at <http://ieeexplore.ieee.org>.

Digital Object Identifier 10.1109/JPHOTOV.2017.2692208

Although several groups tried to suppress the decomposition reactions at the rear surface by introducing interfacial layers [4], [11], [12] and at the top surface by optimizing the fabrication process [9], these reactions, especially at the top surface, persist. The decomposition reactions at the top surface lead to the formation of secondary phases such as  $\text{SnSe}_x$  and  $\text{Cu}_x\text{Se}$ . Even though chemical cleanings such as KCN treatment can remove most of these secondary phases [13], [14], the formation and etching of the secondary phases can introduce defects, vacancies, and dangling bonds.

Recently, several studies focused on passivation of the p–n junction in kesterite solar cells by introducing n-type metal oxide layers such as  $\text{Al}_2\text{O}_3$  [15], [16] or  $\text{TiO}_2$  [17] layers between the kesterite absorber and CdS buffer layers which did improve  $V_{OC}$ . The improvement of  $V_{OC}$  using the passivation layers can be explained by reducing the interface recombination by chemical passivation (reduction of interface trap density) and field effect passivation (formation of a fixed charge density and consequently decreasing the charge carrier concentration at the interface). Wu *et al.* introduced an atomic layer deposited (ALD)  $\text{TiO}_2$  layer between a CZTSSe absorber and CdS buffer layer that improved  $V_{OC}$  while short-circuit current ( $J_{SC}$ ) and fill factor (FF) were similar to the unpassivated solar cells. DLCP and CV profiling of the solar cells revealed that the density of states at the interface is lower in passivated solar cells [17]. Lee *et al.* used an ALD-coated  $\text{Al}_2\text{O}_3$  layer between a high-quality  $\text{Cu}_2\text{ZnSnS}_4$  (CZTS) absorber layer and CdS. In addition, they replaced the intrinsic ZnO in the standard transparent conducting oxide (TCO) stack of indium tin oxide/ZnO with the ALD-coated  $\text{Al}_2\text{O}_3$  layer. It was shown that together these ALD-coated  $\text{Al}_2\text{O}_3$  layers improve  $V_{OC}$ , FF, long-wavelength collection efficiency, and  $J_{SC}$  of the passivated solar cells, resulting in enhanced power conversion efficiencies [16]. Erkan *et al.* also used an ALD-coated  $\text{Al}_2\text{O}_3$  layer between a CZTSSe absorber layer and CdS layer. It was shown statistically that the passivated solar cells have higher  $V_{OC}$ , almost similar  $J_{SC}$  and lower FF as compared to the unpassivated solar cells [15]. However, in general the passivated and unpassivated CZTSSe solar cells in their study had lower performance than the state of the art especially due to low FF. Moreover, it is known that the  $\text{Al}_2\text{O}_3$  layer can be etched during the  $\text{NH}_4\text{OH}$ -containing chemical bath deposition (CBD) of CdS and the etching rate depends on the concentration of  $\text{NH}_4\text{OH}$  basic etchant and the temperature [18]. Thus, depending on the CBD conditions, the impact of  $\text{Al}_2\text{O}_3$  passivation layer can be different.  $\text{TiO}_2$  passivation layer is more stable in the basic CBD environment; however, it might have some drawbacks such as high resistivity and nonoptimal band alignment with the absorber layer that can suppress the charge transport. Therefore, it is very important to control the thickness of the passivation layer to minimize these effects. Using the ALD technique, it is possible to deposit ultrathin layers with controlled thickness but this technique is not widely available, is expensive, and can be time-consuming.

In this study, we used an easy and fast route to create a  $\text{TiO}_2$  interfacial layer by using titanium dioxide dispersion in ethanol [19]. To reduce the series resistivity and make it possible for electrons to tunnel through the  $\text{TiO}_2$  layer, a chemical etching

TABLE I  
OVERVIEW OF THE FABRICATION STEPS REQUIRED TO FABRICATE MODIFIED CZTSE SOLAR CELLS WITH CLOSED AND OPEN  $\text{TiO}_2$  LAYERS

Step	Description
1	Cleaning of $5 \times 5 \text{ cm}^2$ Mo-coated soda lime glass substrates with $\text{NH}_4\text{OH}$ /deionized water
2	E-beam evaporation
3	Selenization in 10% $\text{H}_2\text{Se}$ in $\text{N}_2$ at 460 °C
4	2 min KCN treatment
5	Deposition of closed $\text{TiO}_2$ by spin coating
6	2 min KCN treatment only for samples with open $\text{TiO}_2$ layer
7	CBD CdS deposition
8	(i-)ZnO/Al-ZnO window sputtering
9	Lateral scribing of $0.5 \text{ cm}^2$ solar cells
10	Annealing in $\text{N}_2$ at 200 °C for 1 h

using KCN was done which led to the partial etching of the  $\text{TiO}_2$  layer and creation of openings as confirmed by transmission electron microscopy (TEM) measurements. Passivation layers with nanosized openings are beneficial since the interface can be partially passivated while the photogenerated carriers can be collected by use of the lateral openings. Passivation layers with nanosized point openings have been already used in thin film solar cells including  $\text{Cu}(\text{In,Ga})\text{Se}_2$  [20]–[24] (and references therein) and CZTS [12] solar cells. Techniques such as e-beam lithography [12], [22] have been used to create the nanosized openings through the passivation layers.

## II. EXPERIMENTAL

The processing steps of the modified CZTSe solar cells are shown in Table I. CZTSe absorber layers were prepared by a two-step approach including e-beam deposition of Sn(310 nm)/Zn(150 nm)/Cu(160 nm) stack precursors followed by selenization in 10%  $\text{H}_2\text{Se}$  gas in the  $\text{N}_2$  atmosphere using a rapid thermal processing system. Standard CZTSe solar cells were processed after KCN treatment, CBD of CdS buffer layer, sputtering of i-ZnO/Al-ZnO, and e-beam evaporation of Ni–Al–Ni. In modified solar cells, a layer of  $\text{TiO}_2$  was deposited on top of the CZTSe absorber layer after KCN etching and before the CdS deposition.

In the modified CZTSe solar cells, we used two types of  $\text{TiO}_2$  layers and named as 1) closed and 2) open  $\text{TiO}_2$  layers. To deposit the closed  $\text{TiO}_2$  layer, an ethanol-based solution (sol-gel) was spin coated with 1000 r/min, 5000 r/min/ $\text{s}^2$  for 60 s. The closed  $\text{TiO}_2$  layer is ready directly after the coating in room temperature and does not need any further treatment. This  $\text{TiO}_2$  sol-gel and its physical and chemical properties are explained in more details in [19]. The open  $\text{TiO}_2$  layer was deposited in two steps, first, a closed  $\text{TiO}_2$  layer was deposited on the CZTSe absorber layers and then another KCN treatment was performed on the samples.

The KCN treatment includes dipping the samples in a 5 wt% KCN solution in  $\text{H}_2\text{O}$  for 2 min, followed by rinsing the samples in deionized water and drying with an  $\text{N}_2$  gun. We have previously studied the effect of duration of KCN time on our baseline CZTSe solar cells. It was observed that KCN treatment

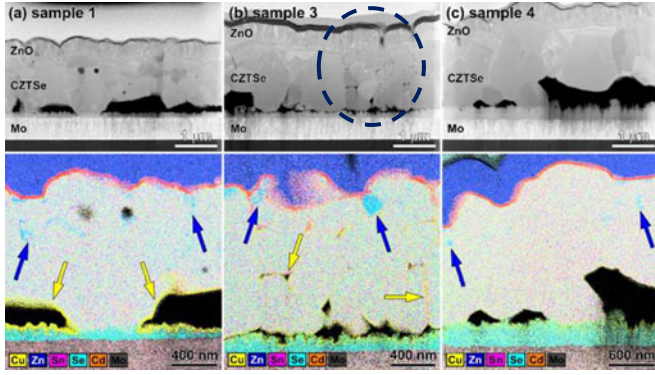


Fig. 1. Overview HAADF-STEM images of the samples (a) 1, (b) 3, and (c) 4. The corresponding STEM-EDX maps are given at the bottom. The bluish areas inside the CZTSe region correspond to the ZnSe inclusions.

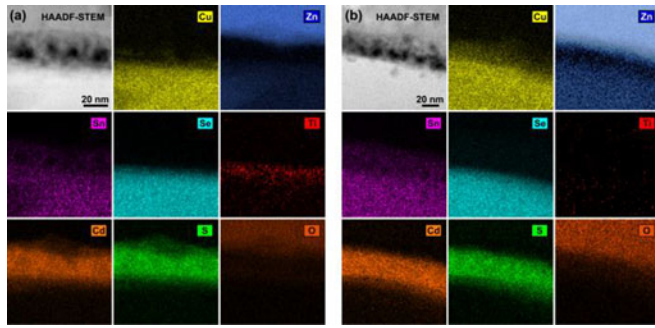


Fig. 2. Elemental EDX maps of (a) sample 1 with closed TiO<sub>2</sub> and (b) sample 4 (without TiO<sub>2</sub>).

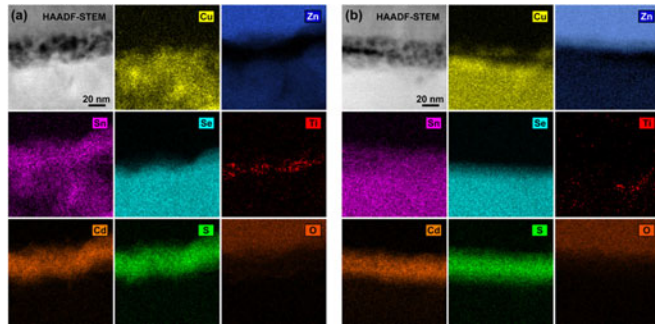


Fig. 3. Elemental EDX maps of sample 3 with open TiO<sub>2</sub> at two different positions (a) and (b).

longer than 2 min led to the lower performance of solar cells due to the surface damage of CZTSe samples [14]. However, in this work, the absorber layer is only affected by the first KCN treatment. The second KCN treatment (after deposition of the TiO<sub>2</sub> layer) mainly affects the TiO<sub>2</sub> and not the CZTSe surface beneath, as can be seen from the TEM analysis given below.

Solar cells were annealed in N<sub>2</sub> atmosphere at 200 °C for 1 h and all the characterizations reported here are performed after this postannealing step.

High angle annular dark field scanning TEM (HAADF-STEM) images and energy dispersive X-ray (EDX) maps were acquired using an FEI Osiris microscope and Titan<sup>3</sup> microscope equipped with a Super-X detector and operated at 200 kV. EDX maps are generated from the intensity of the Mo–K, Se–K,

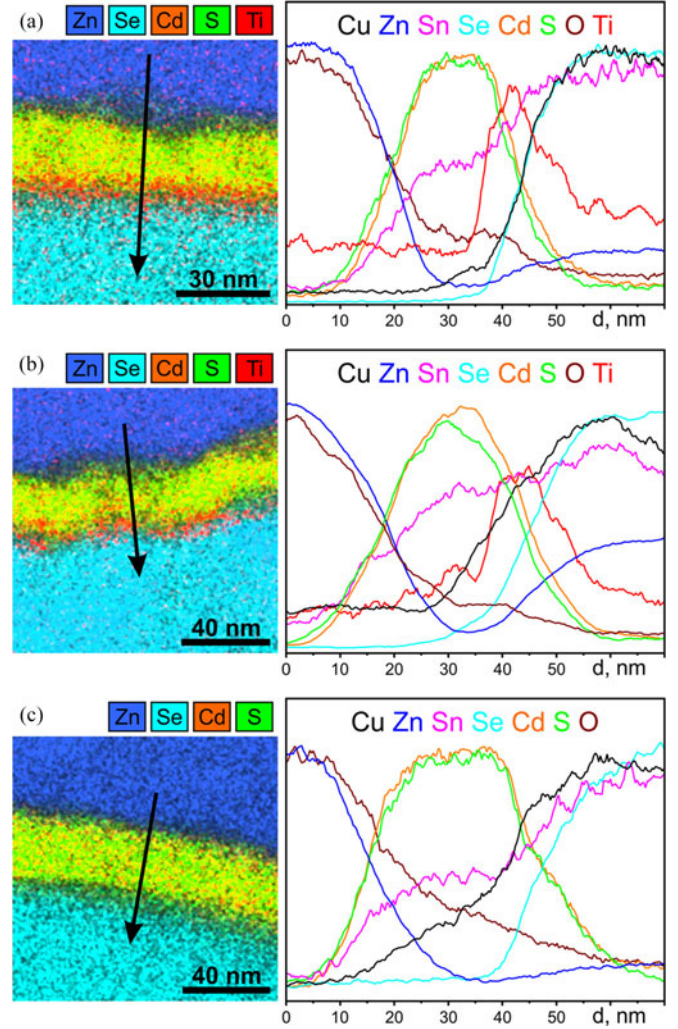


Fig. 4. Mixed map of elements and line profile measured perpendicular to the interface of (a) sample 1 with closed TiO<sub>2</sub>, (b) sample 3 with open TiO<sub>2</sub> in a region where Ti exists, and (c) sample 4 without TiO<sub>2</sub>.

Cu–K, Cd–L, Zn–K, Sn–L, S–K, Ti–K, O–K, C–K lines. The spectra for TEM were prepared using the focused ion beam technique, on a Be support.

In this study, we present the results of one sample with closed TiO<sub>2</sub> (as named sample 1), four samples with open TiO<sub>2</sub> (samples 3, 5, 7, and 9), and their references (samples 2, 4, 6, 8, and 10). Each sample includes at least 12 solar cells and samples with the TiO<sub>2</sub> layer (sample *i*, *i* = 1, 3, 5, 7, and 9) were prepared along with their references (sample *I* + 1) at the same processing condition to exclude the effect of irreproducibility of the fabrication process.

### III. RESULTS AND DISCUSSION

#### A. Characterization of CZTSe Solar Cells With Modified p–n Junction

Overview HAADF-STEM images and STEM-EDX maps of the samples 1 (with closed TiO<sub>2</sub>), 3 (open TiO<sub>2</sub>), and 4 (reference of sample 3) are shown in Fig. 1. The thickness of the CdS layer is around 28 nm in sample 1 and around 30 nm in samples

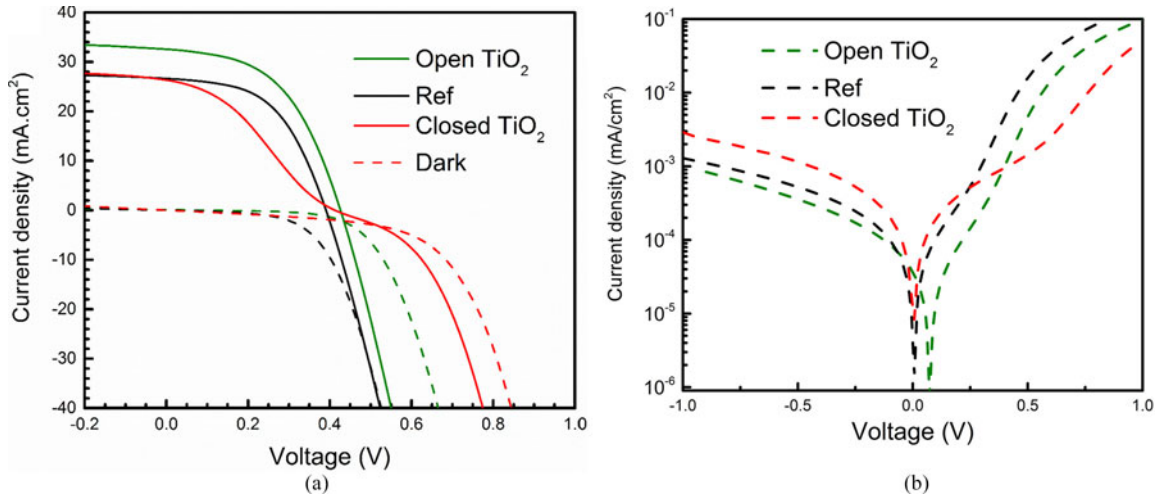


Fig. 5. Illuminated and dark  $J$ - $V$  curves of the best solar cells of sample 1 with closed  $\text{TiO}_2$ , sample 3 with open  $\text{TiO}_2$ , and sample 4 without  $\text{TiO}_2$  (a). Semilog plot of the same dark  $J$ - $V$  curves (b).

TABLE II  
CELL PARAMETERS OF THE BEST SOLAR CELLS OF SAMPLES WITH CLOSED  $\text{TiO}_2$ , OPEN  $\text{TiO}_2$ , AND THE REFERENCE

Solar cell	$J_{SC}$ ( $\text{mA}/\text{cm}^2$ )	$V_{OC}$ (mV)	FF (%)	PCE (%)	$R_s$ ( $\Omega \cdot \text{cm}^2$ )
1-Closed $\text{TiO}_2$	26.2	425	31.7	3.5	2.6
3-Open $\text{TiO}_2$	32.5	426	50.0	6.9	1.7
4-Ref	26.6	391	51.9	5.4	1.9

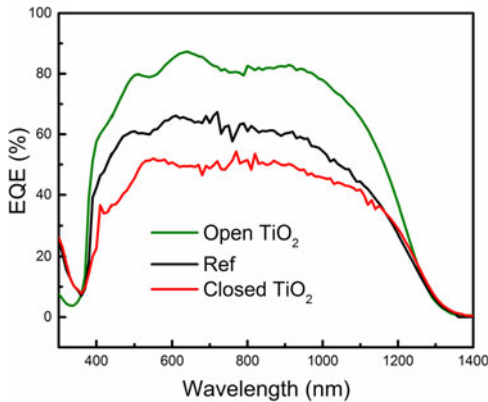


Fig. 6. EQE measurements of the best solar cells of sample 1 (with closed  $\text{TiO}_2$ ), 3 (with open  $\text{TiO}_2$ ), and 4 (reference).

3 and 4. The bluish areas on the STEM-EDX maps correspond to the occurrence of  $\text{ZnSe}$  grains. According to the STEM-EDX analysis a layer of  $\text{MoSe}_2$  ( $\sim 200$ – $300$  nm) and on top of it a thin layer of copper selenide exists at the rear interface, in all samples. Note that in the samples 1 and 4, the CZTSe grains are densely packed. However, there are two different regions in sample 3, one consists of big and densely packed grains and the other region consists of small grains (inside the dashed circle). According to the STEM-EDX analysis, there is a 10–30 nm layer of copper and/or cadmium sulphide segregated at the grain boundaries of this region of sample 3. These segregation of

copper and/or cadmium sulphide might happen during the CBD of CdS through the pin holes in the absorber layer. In sample 1, the segregation of copper sulphide was only observed at the bottom part of the CZTSe layer. No segregation was observed in the sample 4. The composition of 14 individual CZTSe grains of samples 1, 3, and 4 was measured and in samples 1, 3, and 4 the composition is found to be  $\text{Cu}_{1.98(6)}\text{Zn}_{1.17(4)}\text{Sn}_{0.90(2)}\text{Se}_{3.95(9)}$ ,  $\text{Cu}_{2.05(8)}\text{Zn}_{1.13(6)}\text{Sn}_{0.87(4)}\text{Se}_{3.95(10)}$ , and  $\text{Cu}_{2.06(7)}\text{Zn}_{1.13(5)}\text{Sn}_{0.91(9)}\text{Se}_{3.91(7)}$ , respectively.

High magnification TEM and composition profile analysis of these samples were performed at the CZTSe/CdS/ZnO interface. HAADF-STEM images and individual elemental maps of sample 1 with closed  $\text{TiO}_2$  and sample 4 (reference of samples 3) are shown in Fig. 2(a) and (b), respectively. We performed six EDX maps from different positions of sample 1 and a layer of Ti was found in all measurements, an example is shown in Fig. 2(a). We also performed six EDX maps of sample 3 with an open  $\text{TiO}_2$  layer. A layer of Ti was found in two EDX maps of this sample, one of them is shown in Fig. 3(a). However, in the other four EDX maps of this sample, we could not find a continuous layer of Ti, as one shown in Fig. 3(b). Based on these EDX measurements, we conclude that in the open  $\text{TiO}_2$  layer there are some openings in certain regions [see Fig. 3(b)] while the closed  $\text{TiO}_2$  layer is continuous. Fig. 4(a) shows the EDX compositional profile of sample 1 with closed  $\text{TiO}_2$  layer. The same characterization is shown in Fig. 4(b) for sample 3 which has an open  $\text{TiO}_2$  layer in a region where Ti exists and Fig. 4(c) for sample 4 which has no  $\text{TiO}_2$  layer. Note that the peaks of Cd-L (3.13 keV) and Sn-L (3.44 keV) are very close giving an unavoidable erroneous presence of Sn in the CdS layer.

### B. Electrical Analysis of CZTSe Solar Cells With Modified $p$ - $n$ Junction

Fig. 5(a) shows the current–voltage ( $J$ - $V$ ) curves of the champion solar cells of sample 1 (closed  $\text{TiO}_2$ ), sample 3 (open  $\text{TiO}_2$ ), and its reference sample 4. Also Fig. 5(b) shows the semilog plot of the same dark  $J$ - $V$  curves. Solar cell parameters of these

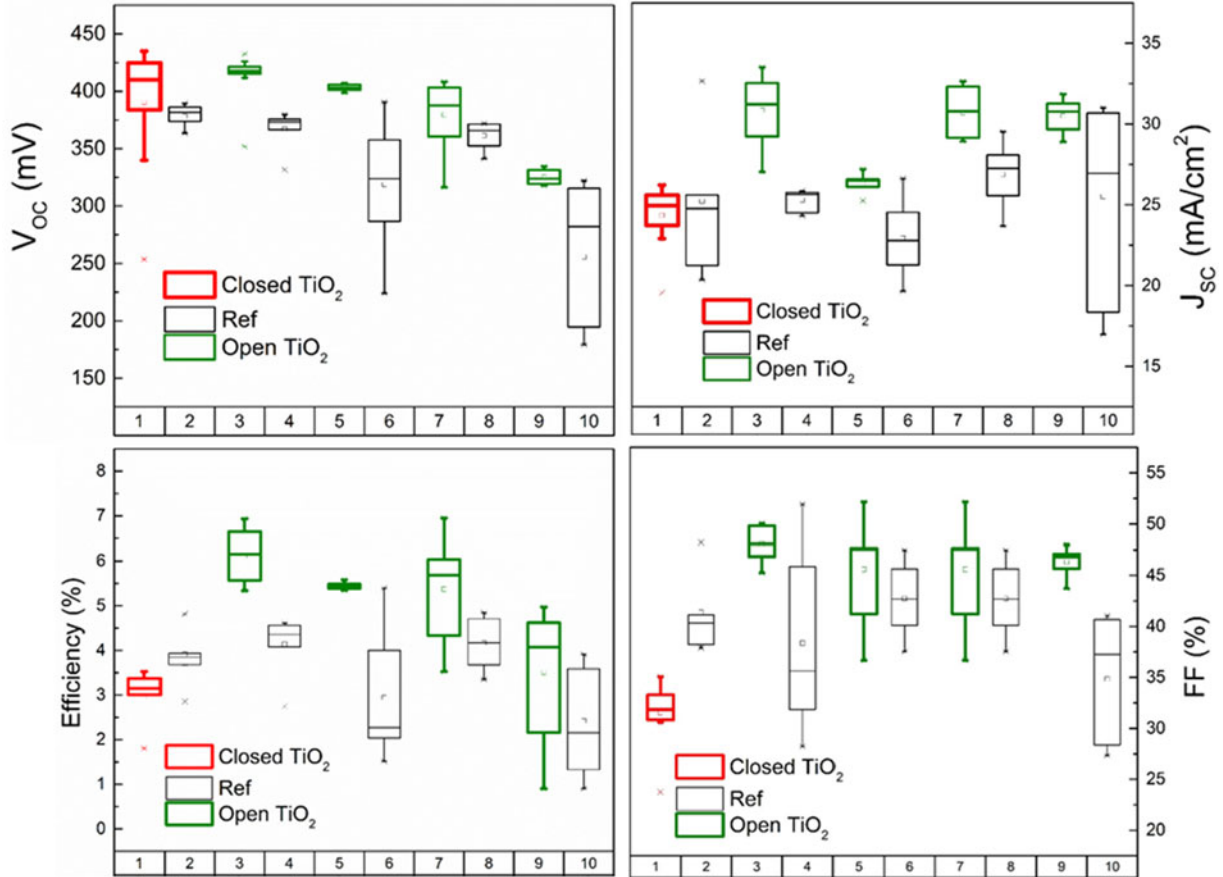


Fig. 7. Electrical parameters of the samples with closed TiO<sub>2</sub>/open TiO<sub>2</sub> layer (red/green boxes) and their references (black boxes). Each box represents values measured from samples containing at least 12 solar cells.

samples are also summarized in Table II. The  $J$ - $V$  curve of the champion solar cell of sample 2 which is the reference of sample 1 is not shown in Fig. 5(a) as it was very similar to sample 4 (see Fig. 7). It can be observed that  $V_{OC}$  is  $\sim 35$  mV higher in solar cells with TiO<sub>2</sub> layers (both open and closed types). However, the  $J$ - $V$  curve of the sample with closed TiO<sub>2</sub> has a kink anomaly and FF is very low. This kink behavior might be attributed to a high positive conduction band offset at the absorber/buffer junction. A high positive offset ( $>0.4$  eV) can be a barrier for the photogenerated electrons. When the recombination velocity is low in the junction (due to the passivation of defects) and there is a positive offset at the junction, the photogenerated electrons accumulate at the junction. At a high forward bias, the accumulated electrons flow back to the absorber layer and recombine there. On the other hand, when the recombination velocity is high, which is the case in standard CZTSe solar cells, the electrons can recombine at the junction at an intermediate forward voltage [25]. By introducing a KCN etching after deposition of TiO<sub>2</sub> in sample 3 with an open TiO<sub>2</sub> layer,  $J_{SC}$  is improved. Moreover, FF is improved to match that value of the reference solar cell. Based on the TEM analysis, the improvement of solar cells with open TiO<sub>2</sub> layer can be attributed to the formation of openings that facilitates the charge transport through the open TiO<sub>2</sub> layer. Series resistance ( $R_s$ ) is slightly higher in samples with TiO<sub>2</sub> layer. This increased resistance can

be attributed to the TiO<sub>2</sub> layer and it is more pronounced in solar cells with a closed TiO<sub>2</sub> layer as compared to solar cells with an open TiO<sub>2</sub> layer which may have a lower thickness and lateral openings.

Fig. 6 shows the external quantum efficiency (EQE) of champion solar cells of sample 1 (closed TiO<sub>2</sub>), sample 3 (open TiO<sub>2</sub>), and reference sample 4. The EQE measurements indicate that collection of photogenerated carriers is improved in the whole region of the spectrum and especially at the long wavelength region. This improvement can be attributed mainly to the passivation of defects at the CZTSe/CdS junction and reduction of recombination currents.

Fig. 7 illustrates the solar cell parameters of several samples including sample 1 with closed TiO<sub>2</sub> layer (red boxes), samples 3, 5, 7, and 9 with open TiO<sub>2</sub> layer (green boxes), and their corresponding references 2, 4, 6, 8, and 10 (black boxes). It can be concluded statistically that by introducing a TiO<sub>2</sub> interfacial layer at the junction,  $V_{OC}$  improved.  $J_{SC}$ , FF, and the conversion efficiency are also statistically higher in solar cells with open TiO<sub>2</sub> layer as compared to their reference solar cells.

#### IV. CONCLUSION

A few studies already reported on the passivation of kesterite solar cells by introducing ALD-coated TiO<sub>2</sub> and Al<sub>2</sub>O<sub>3</sub> layers

between the kesterite absorber layer and CdS buffer layer. Here, by using a solution processed TiO<sub>2</sub> layer, a significant improvement of  $V_{OC}$  was observed; however, a kink anomaly appeared in samples with as deposited TiO<sub>2</sub> layer. This kink anomaly that severely degrades the FF might be attributed to a high barrier at the conduction band. By introducing an additional KCN treatment after spin coating of the TiO<sub>2</sub> layer, the kink anomaly vanished, short-circuit current improved, and FF also improved to match that of the reference solar cells. EDX mappings of the p–n junction using cross-sectional TEM indicated that in samples with as deposited TiO<sub>2</sub>, there is a continuous layer of Ti at the junction while in samples with KCN treatment after deposition of TiO<sub>2</sub>, the Ti layer is not continuous and there are openings at the junction. These openings at the TiO<sub>2</sub> interfacial layer can facilitate the charge carrier transport through this layer. Thus, in addition to the beneficial effect of the passivation and reduction of recombination currents, the charge transport becomes easier through these openings in the interfacial layer. With a CZTSe/CdS/TiO<sub>2</sub>/(KCN treatment)/TCO fabrication process, the best efficiency of 6.9% was achieved as compared to the CZTSe/CdS/TCO baseline process for which 5.4% efficiency was achieved.

#### REFERENCES

- [1] J. P. Leitão *et al.*, “Study of optical and structural properties of Cu<sub>2</sub>ZnSnS<sub>4</sub> thin films,” *Thin Solid Films*, vol. 519, no. 21, pp. 7390–7393, 2011.
- [2] T. Gokmen, O. Gunawan, T. K. Todorov, and D. B. Mitzi, “Band tailing and efficiency limitation in kesterite solar cells,” *Appl. Phys. Lett.*, vol. 103, no. 2013, pp. 103506–103511, 2013.
- [3] K. Wang *et al.*, “Thermally evaporated Cu<sub>2</sub>ZnSnS<sub>4</sub> solar cells,” *Appl. Phys. Lett.*, vol. 97, no. 14, pp. 2–5, 2010.
- [4] S. Ranjbar *et al.*, “Improvement of kesterite solar cell performance by solution synthesized MoO<sub>3</sub> interfacial layer,” *Phys. Status Solidi A*, vol. 6, no. 1, pp. 1–6, 2016.
- [5] R. Haight *et al.*, “Band alignment at the Cu<sub>2</sub>ZnSn(S<sub>x</sub>Se<sub>1-x</sub>)<sub>4</sub>/CdS interface,” *Appl. Phys. Lett.*, vol. 98, no. 25, pp. 253502–253504, 2011.
- [6] T. Minemoto *et al.*, “Theoretical analysis of the effect of conduction band offset of window/CIS layers on performance of CIS solar cells using device simulation,” *Sol. Energy Mater. Sol. Cells*, vol. 67, nos. 1–4, pp. 83–88, 2001.
- [7] J. J. Scragg *et al.*, “A detrimental reaction at the molybdenum back contact in Cu<sub>2</sub>ZnSn(S,Se)<sub>4</sub> thin-film solar cells,” *J. Amer. Chem. Soc.*, vol. 134, no. 47, pp. 19330–19333, 2012.
- [8] J. J. Scragg *et al.*, “Effects of back contact instability on Cu<sub>2</sub>ZnSnS<sub>4</sub> devices and processes,” *Chem. Mater.*, vol. 25, no. 15, pp. 3162–3171, 2013.
- [9] A. Weber, R. Mainz, and H. W. Schock, “On the Sn loss from thin films of the material system Cu–Zn–Sn–S in high vacuum,” *J. Appl. Phys.*, vol. 107, no. 1, pp. 013516–013521, 2010.
- [10] J. Li *et al.*, “The band alignment at CdS / Cu<sub>2</sub>ZnSnSe<sub>4</sub> heterojunction interface,” *Surf. Interface Anal.*, vol. 45, pp. 682–684, 2013.
- [11] S. Lopez-Marino *et al.*, “Inhibiting the absorber/Mo-back contact decomposition reaction in Cu<sub>2</sub>ZnSnSe<sub>4</sub> solar cells: the role of a ZnO intermediate nanolayer,” *J. Mater. Chem. A*, vol. 1, no. 29, pp. 8338–8343, 2013.
- [12] B. Vermang *et al.*, “Rear surface optimization of CZTS solar cells by use of a passivation layer with nanosized point openings,” *IEEE J. Photovolt.*, vol. 6, no. 1, pp. 332–336, Jan. 2016.
- [13] M. Buffière *et al.*, “KCN chemical etch for interface engineering in Cu<sub>2</sub>ZnSnSe<sub>4</sub> solar cells,” *ACS Appl. Mater. Interfaces*, vol. 7, no. 27, pp. 14690–14698, Jul. 2015.
- [14] S. Sahayaraj *et al.*, “Effect of the duration of a wet KCN etching step and post deposition annealing on the efficiency of Cu<sub>2</sub>ZnSnSe<sub>4</sub> solar cells,” *Thin Solid Films*, 2016, doi: 10.1016/j.tsf.2016.09.055.
- [15] M. E. Erkan, V. Chawla, and M. A. Scarpulla, “Reduced defect density at the CZTSSe/CdS interface by atomic layer deposition of Al<sub>2</sub>O<sub>3</sub>,” *J. Appl. Phys.*, vol. 119, pp. 194504–194511, 2016.
- [16] Y. S. Lee *et al.*, “Atomic layer deposited aluminum oxide for interface passivation of Cu<sub>2</sub>ZnSn(S,Se)<sub>4</sub> thin-film solar cells,” *Adv. Energy Mater.*, vol. 6, no. 12, pp. 1–5, 2016.
- [17] W. Wu *et al.*, “Characterization of CZTSSe photovoltaic device with an atomic layer-deposited passivation layer,” *Appl. Phys. Lett.*, vol. 105, no. 4, pp. 042108–042111, 2014.
- [18] J. Oh, J. Myoung, J. S. Bae, and S. Lim, “Etch behavior of ALD Al<sub>2</sub>O<sub>3</sub> on HfSiO and HfSiON stacks in acidic and basic etchants,” *J. Electrochem. Soc.*, vol. 158, no. 4, pp. D217–D222, 2011.
- [19] A. Hadipour, R. Müller, and P. Heremans, “Room temperature solution-processed electron transport layer for organic solar cells,” *Org. Electron.*, vol. 14, no. 10, pp. 2379–2386, 2013.
- [20] P. Reinhard *et al.*, “Alkali-templated surface nanopatterning of chalcogenide thin films: A novel approach toward solar cells with enhanced Efficiency,” *Nano Lett.*, vol. 15, pp. 3334–3340, 2015.
- [21] R. Kotipalli *et al.*, “Investigating the electronic properties of Al<sub>2</sub>O<sub>3</sub>/Cu(In,Ga)Se<sub>2</sub> interface,” *AIP Adv.*, vol. 5, no. 10, pp. 107101–107106, 2015.
- [22] B. Vermang *et al.*, “Introduction of Si PERC rear contacting design to boost efficiency of Cu(In,Ga)Se<sub>2</sub> solar cells,” *IEEE J. Photovolt.*, vol. 4, no. 6, pp. 1644–1649, Nov. 2014.
- [23] B. Vermang *et al.*, “Employing Si solar cell technology to increase efficiency of ultra-thin Cu(In,Ga)Se<sub>2</sub> solar cells,” *Prog. Photovolt. Res. Appl.*, vol. 22, pp. 1023–1029, 2014.
- [24] B. Vermang, V. Fjällström, J. Pettersson, P. Salomé, and M. Edoff, “Development of rear surface passivated Cu(In, Ga)Se<sub>2</sub> thin film solar cells with nano-sized local rear point contacts,” *Sol. Energy Mater. Sol. Cells*, vol. 117, pp. 505–511, 2013.
- [25] R. Scheer and H. Schock, *Chalcogenide Photovoltaics Physics, Technologies, and Thin Film Devices*. Hoboken, NJ, USA: Wiley, 2011.

Authors’ photographs and biographies not available at the time of publication.